Computational methods based on X-ray microtomography for quantitative analysis of lyophilized products

Proceedings of Eurodrying'2019
Torino, Italy, July 10-12, 2019

Paper 138

COMPUTATIONAL METHODS BASED ON X-RAY MICROTOMOGRAPHY FOR QUANTITATIVE ANALYSIS OF LYOPHILIZED PRODUCTS

Luigi C. Capozzi, Antonello A. Barresi, Giorgia Montalbano, Chiara Viatale-Brovarone, and Roberto Pisano

Department of Applied Science and Technology, Politecnico di Torino
24 corso Duca degli Abruzzi, Torino, Italy, 10129
Tel.:+39-(0)11-090-4679,
E-mail: roberto.pisano@polito.it

Abstract

In this work, X-ray microcomputed tomography is used to analyse and reconstruct the inner structure of lyophilized products. Various computational methods were used to determine the structural parameters that impact on mass transport of vapor during drying, i.e., pore size, tortuosity, and permeability. These methods include slice-by-slice 2D image analysis of the entire sample, 3D image analysis of small portions of the product and CFD simulations.

Keywords*: Freeze-drying/lyophilization, micro-CT, image analysis, CFD simulations*

1 Introduction

Freeze-drying is a gentle drying method used in the pharmaceutical industry for producing high-value drugs. The process starts out with the freezing of liquid solutions, the drying via solvent sublimation and ends with a desorption step. Pharmaceutical freeze-drying is facing a period of significant changes due to new emerging technologies and because the more and more stringent requirements set by the regulatory authorities. Product quality and its control has become the most important input of these changes (Capozzi et al., 2019c). Since many years, freeze-drying community is moving towards a more accurate control of product quality and process control; in this perspective, the control of freezing step is fundamental for designing products with the desired characteristics and manage variability. In fact, freezing determines many characteristics of the final product such as the cake structure, the polymorph composition, and the stability of many APIs, influences the drying rate and the final moisture content. The freezing step is also responsible for the batch-to-batch, vial-to-vial and the intra-vial variability in product characteristics.

In the last few years, the lyophilization community has put many efforts in controlling the freezing and studying the relationship between freezing protocols and product characteristics (Oddone *et al.*, 2016; Capozzi and Pisano, 2018). The knowledge of the internal structure is crucial to better understand the relationship between freezing and intra-vial heterogeneity, as well as between freezing and drying behaviour of the product being lyophilized.

X-ray microcomputed tomography (micro-CT) is emerging as an effective imaging technique for studying the structure of the lyophilized product and as an inspection tool (Mousavi *et al.*, 2007; Izutsu *et al.*, 2014; Parker *et al.*, 2010; Pisano *et al.*, 2017; Goshima *et al.,* 2016; Haeuser *et al.*, 2018). On the other hand, micro-CT analysis requires computational methods for having a quantitative estimation of product characteristics. Image segmentation (Capozzi *et al.*, 2018; Arsiccio *et al.*, 2019), frequency domain image analysis and artificial

neural network (Grassini *et al.*, 2016) were recently proposed as computational methods to be coupled to imaging analysis.

In this work, X-ray microcomputed tomography is used to analyze and reconstruct the structure of the porous product. Various computational methods were used to determine the structural parameters that impact on mass transport of vapor during drying, i.e., pore size, tortuosity, and permeability. These methods included:

(i) slice-by-slice 2D image analysis of the entire sample;

(ii) 3D image analysis of small portions of the product (the so-called representative elementary volume, REV) sampled at different heights along the product;

(iii) CFD simulations applied to REVs at different heights in the products.

2 Material and method

2.1 Production of lyophilized products

Samples were lyophilized in the LyoBeta 25 freeze-dryer (Telstar, Terrassa, Spain) using an aqueous solutions of mannitol 5% (w/w) as model formulation. The solutions were prepared using water for injection (Fresenius Kabi Italia, Isola della Scala, Italy) and filtered using 0.2 µm filters. An aliquot of 3 ml of mannitol solution was filled into tubing vials (10R 24.0 x 45.0, Nuova Ompi, Piombino Dese, Italy). The sample were lyophilized using three different configurations/protocols:

a) batch freeze-drying, uncontrolled freezing;
b) suspended-vial freeze-drying, uncontrolled freezing (Capozzi et al., 2019c);
c) suspended-vial freeze-drying, controlled freezing via VISF (Capozzi et al., 2019c).

Those three configurations were used in order to produce products with different structural characteristics; in the configuration (c) nucleation was induced at 268 K.

2.2 Micro-CT analysis

As a first step, the dried sample was analysed using the SkyScan 1272 (Bruker microCT, Kontich, Belgium); X-ray beams were generated by a tungsten filament at 50 kV and 200 µA. Samples were analysed over a rotation range of 180°, with a step of 0.01°, an exposure time of 200 ms per projection and a pixel size of 3 µm. After that, the images obtained were analysed using the computational methods described below.

2.3 Slice-by-slice 2D image analysis

The first computational method developed in this work consists in a 2D image analysis of the whole stack of images produced in a single micro-CT analysis. The open source library for Python *scikit-image* was used for the implementation of three algorithms. All these algorithms give an estimation of the average pore size and permeability, but such calculations are carried out using a different numerical approach. The preliminary operations before implementing the algorithms consisted of acquiring the original images, applying a threshold filter in order to binarize the images and removing the small objects below 70 px, see Fig. 1.

After the algorithms were applied, mean pore diameter (d_p) and permeability (B_0) were calculated using the formulas shown in Table 1. The algorithm (ii) provides an estimation of permeability for each pore within the image, so that average permeability can be calculated considering the pores as parallel channels (Eq.4a) or using a number-weight averaging (Eq. 4b).

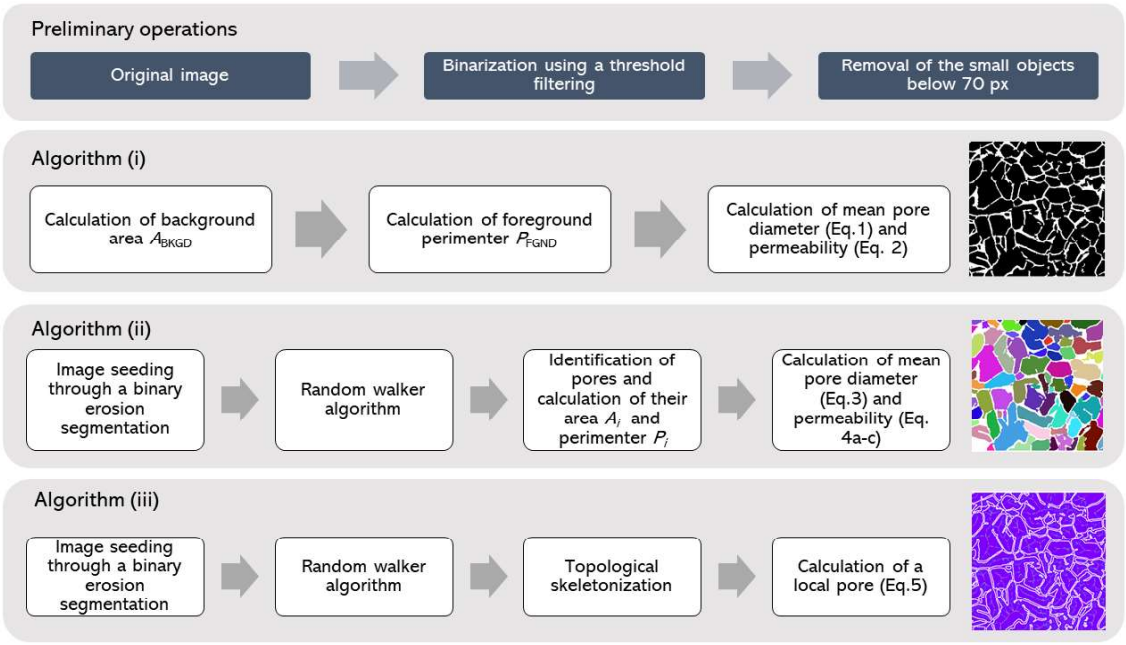

Fig. 1. Preliminary operations and schematic of the three algorithms

Table 1. Calculation of the mean pore diameter and permeability through the three algorithms.

	Mean pore diameter	Permeability
Algorithm (i)	$d_p = \frac{4A_{BKGD}}{P_{FGND}}$ (1)	$B_0 = \frac{d_p^2}{32}$ (2)
Algorithm (ii)	$d_p = \frac{1}{n}\sum_{i=0}^{n}\frac{4A_i}{P_i}$ (3)	$B_{0,i} = \frac{d_{p,i}^2}{32}$ (4a)
		$\langle B_0 \rangle_{\parallel} = \frac{\sum_{i=0}^{n} B_{0,i}A_i}{\sum_{i=0}^{n} A_i}$ (4b)
		$\langle B_0 \rangle_{nw} = \frac{1}{n}\sum_{i=0}^{n} B_{0,i}$ (4c)
Algorithm (iii)	$d_{p,loc}$ (5)	$B_0 = \frac{d_{p,loc}^2}{32}$ (6)

2.4 3D image analysis

The second computational method uses the software BLOB3D developed by Ketcham (2005); this software is specifically designed to measure discrete features such as clasts, grain, voids with particular regard to geological applications, but here is used to analyse the voids in the lyophilized samples. As a first step, the segmentation of the stack of images divided the domains constituted by the voids and the walls. Then, the contiguous sets of voxels are separated so that the interconnected or touching objects become separate discrete features. Finally, the volume and the surface area of each discrete feature is calculated; a mean pore diameter is finally calculated.

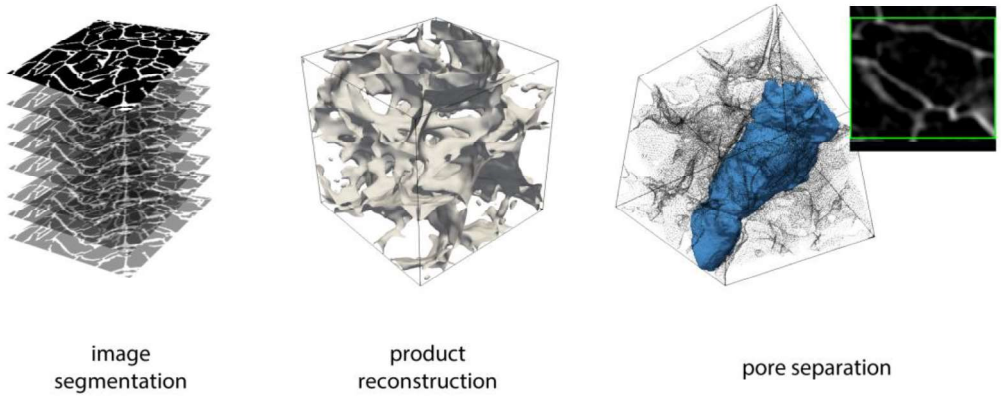

Fig. 2. Workflow of the software Blob3D.

2.5 CFD simulation

Similar to previous works published by the authors (Capozzi *et al.*, 2019a; Capozzi *et al.*, 2019b), CFD simulations were performed in order to estimate tortuosity and permeability. A 3D domain (the so-called REV, relevant element volume) was generated by reconstructing product structure as obtained by the micro-CT analysis. A STL file was generated by using the software Bruker CTvox (Mannheim, Germany). The utilities *blockMesh* and *snappyHexMesh* provided with the open source software OpenFoam 5.0 were used to generate the computational domain, which is the complementary volume respect to the one generated in the STL file, and, after that, the Navier-Stokes equations under Stokes flow were solved within the domain. Similar to Capozzi *et al.* (2019b), successive refinements of the grid were performed until the independence of the solution was reached.

The velocity field obtained from the steady-state solution was used to calculate the tortuosity and permeability as follows,

$$\tau = \frac{\int_{REV} |\mathbf{u}| dV}{\int_{REV} u_z dV} \tag{7}$$

$$B_0 = \mu \left(\frac{\Delta p_z}{L_z} \right)^{-1} \frac{1}{V_{REV}} \int_{REV} u_z dV \tag{8}$$

3 Results and discussion

There exists a strong correlation between freezing protocol and pore dimension. Fig. 3 shows the diameter of pores within the porous cake along the product height. Pore diameter was calculated using both the 2D and 3D image analysis. VISF was able to produce a product with pores in the range of 90-100 µm, with a thin crust at the top surface made of small pores, which are the result of the local supercooling resulting due to the fast evaporation that triggers nucleation. In the case of uncontrolled nucleation, suspended-vial configuration led to a cake with bigger pores than those obtained in the conventional, batch, shelf-ramped freezing.

From Fig. 3 it is clear that there are differences in the values of pore diameter depending on the definition of pore diameter itself. The evaluation of the pore diameter as defined in Eq. 1 seemed not to be consistent as that method predicted almost the same mean pore diameter for the three cases, whereas direct and indirect observation of the products clearly state that these three products possessed very different pore size. The values of pore diameter defined from the medial axis of the topological skeleton (Eq. 5) were smallerr compared to those obtained by defining pore diameter as the area to perimeter ratio (Eq. 3). However, the pore diameter defined as the area to perimeter ratio, also called hydraulic diameter, is based on a purely fluid dynamics definition, as it represents the diameter of an equivalent circular conduit which maintains the same conservation of momentum of the pristine pore. On the other hand, $d_{p,loc}$ seemed to be more coherent with the values found by using the 3D image analysis.

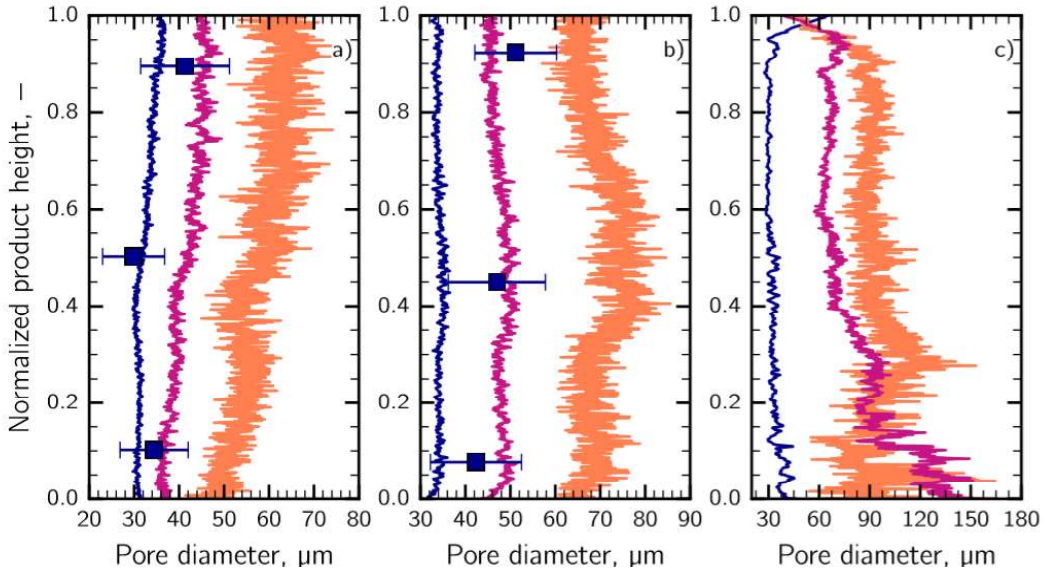

Fig. 3. Mean pore diameter along the product height in the case of (a) batch and uncontrolled nucleation, (b) suspended-vial configuration and uncontrolled nucleation, (c) suspended-vial configuration and VISF. Data refer to algorithm i) (blue lines, Eq. 1), algorithm ii) (orange lines, Eq. 3) and algorithm iii) (violet lines, Eq. 5); 3D image analysis data are also reported(blue dots).

As shown in Fig. 4, the tortuosity as evaluated by using CFD simulations ranged between 1.2 and 1.4. These values are smaller than those obtained by Goshima *et al.* (2016), where tortuosity was found to be 2-3; it has to be pointed out that the approach of Goshima *et al.* (2016) is based on the image analysis of longitudinal sections of the lyophilized cake, and so on pure geometrical basis.

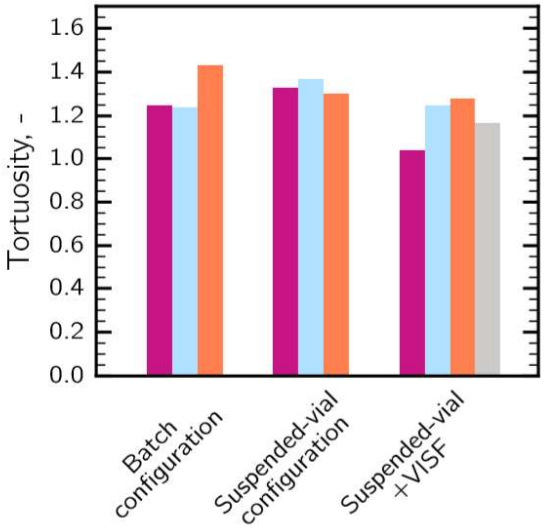

Fig 4. Tortuosity evaluated using CFD simulation in the case of batch and suspended-vial configuration (uncontrolled nucleation) and in the case of VISF applied to suspended-vial configuration. Bars refer to different positions in the product: (violet) bottom, (sky-blue) centre, (oranges) top, (grey) top crust.

Finally, the permeability coefficient of the porous cake was evaluated using both image analysis and CFD simulations, see Fig. 5. The evaluation of permeability from image analysis and Eq. 4b, supposes that each slice in the porous cake is constituted of parallel pores of different size, whereas Eq. 4c is based on a pure arithmetic average. On the other hand, the permeability as calculated from CFD simulations takes into account the real structure of the pore medium. Anyway, Fig. 5 shows that the two approaches result in comparable values.

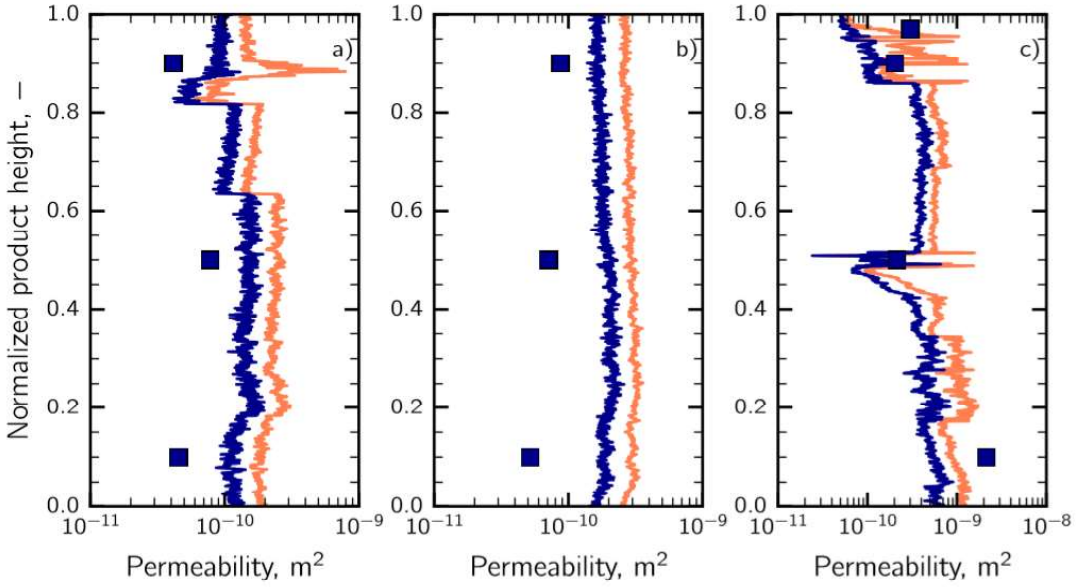

Fig 5. Permeability along the product height in the case of the (a) batch ad uncontrolled nucleation, (b) suspended-vial configuration and uncontrolled nucleation and (c) suspended-vial configuration and VISF. Data refer to (blue lines) Eq. 4b, (orange lines) Eq. 4c, (blue dots) CFD simulations.

4 Conclusions

X-ray microcomputed tomography was used to analyse and reconstruct the structure of the porous product. Various computational methods were used to determine the structural parameters that impact on mass transport of vapor during drying, i.e., pore size, tortuosity, and permeability. It has been shown that these methods can give different results according to the definition of the structural parameters. The present work pointed out the difficulties arising in determining the structural properties of such complex systems and calls for further studies on this topic.

List of symbols

A	area, m^2
B_0	permeability coefficient, m^2
d_p	pore diameter, m
$d_{p,loc}$	local pore diameter from image skeletonization, m
L_z	REV length, m
P	perimeter, m
Δp_z	pressure drop in the z-direction through the REV, Pa
$\mathbf{u}$	velocity vector, ms^{-1}
u_z	velocity in the z-direction through the REV, ms^{-1}
V	REV volume, m^3
Greek letters	
μ	viscosity of gas mixture, kg m^{-1} s^{-1}
τ	tortuosity, -
Subscript	
$\|\|$	parallel model
BKGD	background
FGND	foreground
nw	number weight

Acknowledgments

Computational resources were provided by ISCRA-Cineca HPC CLASS-C Grants HP10COMJ35.

References

Arsiccio A., Sparavigna A.C., Pisano R. and Barresi A.A., 2019, Measuring and predicting pore size distribution of freeze-dried solutions. *Drying Technol.* **37**(4), 435_447.

Capozzi L.C. and Pisano R., 2018, Looking inside the 'black box': Freezing engineering to ensure the quality of freeze-dried biopharmaceuticals. *European Journal of Pharmaceutics and*

Biopharmaceutics, 129, pp.58-65.

Capozzi L.C., Arsiccio A., Sparavigna A.C., Pisano R. and Barresi A.A., 2018, Image segmentation and 3D reconstruction for improved prediction of the sublimation rate during freeze drying. *IDS'2018 – Proc. 21st International Drying Symposium*, Valencia, Spain, 11-14 September 2018. Editorial Universitat Politècnica de València, Valencia, Spain, pp. 411-418.

Capozzi L. C., Barresi A. A. and Pisano R., 2019a, A multi-scale computational framework for modeling the freeze-drying of microparticles in packed-beds. *Powder Technol.* **343**, 834-846.

Capozzi L. C., Barresi A. A. and Pisano R., 2019b, Supporting data and methods for the multi-scale modelling of freeze-drying of microparticles in packed-beds. *Data Brief* **22**, 722-755.

Capozzi L., Trout B. and Pisano R., 2019c, From batch to continuous: Freeze-drying of suspended vials for pharmaceuticals in unit-doses. *Ind. Eng. Chem. Res.* **58**(4), 1635-1649.

Grassini S., Pisano R., Barresi A.A., Angelini E. and Parvis M., 2016, Frequency domain image analysis for the characterization of porous products. *Measurement* **94**, 515-522.

Goshima H., Do G. and Nakagawa K., 2016, Impact of ice morphology on design space of pharmaceutical freeze-drying. *J. Pharm. Sci.* **105**(6), 1920-1933.

Haeuser C., Goldbach P., Huwyler J., Friess W. and Allmendinger A., 2018, Imaging techniques to characterize cake appearance of freeze-dried products. *J. Pharm. Sci.* **107**(11), 2810-2822.

Izutsu K., Yonemochi E., Yomota C., Goda Y. and Okuda H., 2014, Studying the morphology of lyophilized protein solids using X-ray Micro-CT: Effect of post-freeze annealing and controlled nucleation. *AAPS PharmSciTech* **15**(5), 1181-1188.

Ketcham R. A, 2005, Computational methods for quantitative analysis of three-dimensional features in geological specimens. *Geosphere* **1**(1), 32-41.

Mousavi R., Miri T., Cox P. and Fryer P., 2007, Imaging food freezing using X-ray microtomography. *Int. J. Food Sci. Technol.* **42**(6), 714-727.

Oddone I., Van Bockstal P., De Beer T. and Pisano R., 2016, Impact of vacuum-induced surface freezing on inter- and intra-vial heterogeneity. *Europ. J. Pharm. Biopharm.* **103**, 167-178.

Parker A., Rigby-Singleton S., Perkins M., Bates D., Le Roux D., Roberts C., Madden-Smith C., Lewis L., Teagarden D., Johnson R. and Ahmed S., 2010, Determination of the influence of primary drying rates on the microscale structural attributes and physicochemical properties of protein containing lyophilized products. *J. Pharm. Sci.* **99**(11), 4616-4629.

Pisano R., Barresi A.A., Capozzi L.C., Novajra, G., Oddone I. and Vitale-Brovarone C., 2017, Characterization of the mass transfer of lyophilized products based on X-ray micro-computed tomography images. *Drying Technol.* **35**(8), 933-938.